Accurate and efficient description of interacting carriers in quantum nanostructures by selected configuration interaction and perturbation theory

Moritz Cygorek,[1] Matthew Otten,[2] Marek Korkusinski,[3] and Pawel Hawrylak[1]
[1]*Department of Physics, University of Ottawa, K1N 6N5 Ottawa, Canada*
[2]*Center for Nanoscale Materials, Argonne National Laboratory, Lemont, Illinois 60439, USA*
[3]*National Research Council of Canada, K1A OR6 Ottawa, Canada*

(Received 11 March 2020; revised manuscript received 24 April 2020; accepted 28 April 2020; published 18 May 2020)

We present a method to accurately and efficiently calculate many-body states of interacting carriers in quantum nanostructures based on a combination of iterative selection of configurations and perturbation theory. This method enables investigations of large excitonic complexes and multielectron systems with near full configuration interaction accuracy, even though only a small subspace of the full many-body Hilbert space is sampled, thus saving orders of magnitudes in computational resources. Important advantages of this method are that the convergence is controlled by a single parameter, the threshold, and that ground and excited states can be treated on an equal footing. On the example of InAsP nanowire quantum dots described using a million-atom tight-binding approach, we demonstrate the extreme efficiency of the method by numerical studies of large excitonic complexes filling up to the fourth electronic shell. We find that the method generally converges fast as a function of the threshold, profiting from a significant acceleration due to the perturbative corrections. The role of the choice of single-particle basis states is discussed. It is found that the algorithm converges faster in the Hartree-Fock basis only for highly charged systems, where Coulomb repulsion dominates. Finally, based on the observation that second-order perturbative energy corrections only depend on off-diagonal elements of the many-body Hamiltonian, we present a way to accurately calculate many-body states that requires only a relatively small number of Coulomb matrix elements.

DOI: 10.1103/PhysRevB.101.205308

I. INTRODUCTION

Quantum nanostructures such as quantum dots [1–4], quantum rings [5], and nanoplatelets [6] are workhorse systems for the development of semiconductor-based quantum technology devices, such as single-photon emitters [7–9] or sources of entangled photon pairs [10–13]. Due to the confinement of electrons to a small volume, quantum dots can be viewed as artificial atoms. When two or more atoms are brought together they form molecules. Similarly, more complex devices can be built from quantum dots by fabricating systems with multiple dots that are close enough to introduce interdot tunneling [14–17]. These systems can be used, e.g., to realize two- or three-dot spin qubits [18–21]. Complexity is also added when a quantum dot is loaded with multiple charge carriers [22–25]. In analogy to transition metal elements, occupation of dots with multiple electrons can lead to the formation of correlated magnetic states for partially filled shells [26]. In quantum dots, multiexcitonic complexes [27] are interesting, as they can be easily probed by photoluminescence at high intensities [28–30]. The biexciton is particularly relevant for the generation of entangled photon pairs in the biexciton-exciton cascade [31] and the emission from the lowest-energetic three-exciton complex, which necessarily involves occupation of the p shell, and contains information about the lateral confinement in the quantum dot [32,33]. Similarly, the d and f shells can be probed via the emission of the lowest-energetic states of 7- and 13-exciton complexes, respectively. Charged excitonic complexes such as trions [34,35] can be used for the generation of highly entangled photon cluster states [36,37] that are required for measurement-based quantum computation [38]. The proposal of implementing a synthetic Haldane chain [39], which possesses an exotic quantum phase with a quadruply degenerate symmetry-protected topological ground state protected by a gap, in a quantum dot array with half-filled p-shell states combines the complexities of multiple carriers within one dot with that of multidot systems.

A quantitative theoretical description for such applications is highly desirable. However, the direct numerical calculation of many-body states of multiple interacting carriers in a semiconductor nanostructure is difficult because of the curse of dimensionality, i.e., the fast growth of the many-body Hilbert space $\mathcal{H}$ with the number of carriers and single-particle states. For an excitonic complex composed of n_e electrons and n_h holes distributed on a set of N_e confined electron and N_h hole states, the dimension of $\mathcal{H}$ is $\binom{N_e}{n_e} \times \binom{N_h}{n_h}$. Dozens of single-particle states might be needed in full configuration interaction (CI) calculations [40], as shown in Fig. 1(b), which depicts the positions of the spectral lines emitted from the lowest exciton and biexciton state as a function of the number of single-particle states $N_e = N_h$ for a hexagonal $InAs_{0.2}P_{0.8}$ quantum dot with diameter 18 nm and height 4 nm in a wurtzite InP nanowire [41] as sketched in Fig. 1(a). In particular, relative quantities such as the biexciton binding energy $\Delta E_B = (E_{2X} - E_X) - E_X$ converge slowly because

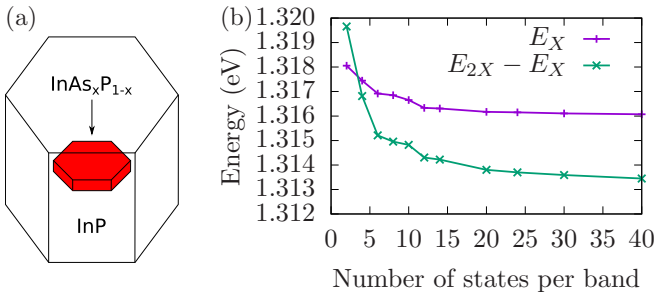

FIG. 1. (a) Hexagonal $InAs_xP_{1-x}$ quantum dot (red) inside a segment of an InP nanowire. (b) Positions of the spectral lines emitted from the lowest biexciton and exciton states as a function of the number of single-particle states in conduction and valence band used in a full CI calculation.

larger complexes generally converge more slowly than smaller complexes.

Therefore, for larger complexes full CI calculations become prohibitively demanding and one has to resort to approximate methods. A common principle of many such approximations is that, in most situations, only a small subspace of the full Hilbert space contributes significantly to the many-body states of interest, e.g., to the ground state. The Hartree-Fock method is a fast and easy approximation that seeks to find the optimal description in terms of a single configuration. It may also help to speed up the convergence of larger CI calculations if they are performed starting from Hartree-Fock single-particle states [42]. If the nanostructure possesses symmetries [43], the full Hilbert space can be decoupled into different blocks, each of which has a much smaller dimension than the full problem. Similarly, one may also exploit hidden symmetries [28,44] to investigate large excitonic complexes. In quantum chemistry, configuration interaction with single and double excitations or coupled cluster approaches [45] are commonly used to calculate many-body states in large Hilbert spaces. Lately, also representations of many-body states in terms of matrix product states have been shown to perform well [46–48], especially for ground states and for one-dimensional systems.

In this paper, we present a general method for the numerical calculation of correlated many-body states in quantum nanostructures that does not require any strong assumption about the wave functions such as particular symmetries and also enables the calculation of excited states. In light of the analogy between quantum dots and atoms, it is suggestive to take inspiration from quantum chemistry. Concretely, we implement a version of the CIPSI (configuration interaction by perturbation with multiconfigurational zeroth-order wave function selected by iterative process) method [49–52] for the solution of problems involving interacting carriers in quantum nanostructures such as quantum dots, and demonstrate its efficiency. This method consists of diagonalizing the many-body Hamiltonian in a reduced space of configurations that are selected iteratively by a criterion based on perturbation theory. After diagonalization in the relevant subspace, the effects of the configurations outside of the selected subspace are accounted for perturbatively. A major advantage of CIPSI is that it is a controlled approximation as there exists a single convergence parameter, the threshold ξ, that controls the accuracy, where the full CI result is obtained in the limit $\xi \to 0$. In quantum chemistry, selected CI methods have been applied to large, strongly correlated molecules, such as the chromium dimer, correlating 28 electrons in 198 orbitals, leading to a total Hilbert space of 10^{42} using 10^9 variational states and 10^{12} perturbative states [53].

Here, we describe the application of the CIPSI method in the context of quantum nanostructures. While typical applications in quantum chemistry aim at an accurate description of a few interacting atoms, modeling quantum nanostructures often involves hundreds of thousands to millions of atoms and the effects due to strain, alloying, and the underlying crystal structure have to be included. These effects are usually accounted for on the level of single-particle states in effective mass approximation, $\mathbf{k}\cdot\mathbf{p}$ theory, or empirical pseudopotentials [54]. To facilitate its general use beyond a specific single-particle calculation method, we formulate the many-body calculation method for arbitrary single-particle states. For concrete examples of InAsP nanowire quantum dots, we obtain single-particle states using a tight-binding based atomistic description [41]. We present numerical calculations to test the accuracy and numerical demands of the selected CI method for multiexciton complexes. We find that the algorithm converges fast as a function of the threshold, so that results with near full CI accuracy are obtained while only a small fraction of configurations of the full Hilbert space has been selected, reducing the numerical demands by many orders of magnitude. A large part of the efficiency of the CIPSI algorithm can be attributed to the perturbative corrections.

We then use the selected CI method to simulate the emission spectra of three-exciton complexes, which requires the calculation of many excited biexciton states. Subsequently, we investigate the role of the choice of the basis of the single-particle states and find that starting from the Hartree-Fock basis can lead to an enhanced convergence for highly charged many-body complexes, but building Slater determinants from eigenstates of a single-particle Hamiltonian turns out to be favorable for charge neutral systems.

Finally, having found that the perturbative corrections are responsible for a large part of the accuracy of the CIPSI algorithm and observing that the perturbative terms only contain off-diagonal matrix elements, we devise a method to accurately calculate many-body states that requires the knowledge of only a small fraction of the Coulomb matrix elements constructed from all single-particle states. This is especially relevant when single-particle states are obtained from atomistic simulations, since the calculation of Coulomb matrix elements is one of the most time-consuming steps in the overall procedure of the simulation of many-body states in quantum nanostructures. Therefore, this approach, which potentially reduces the total number of Coulomb matrix elements by orders of magnitude, is extremely useful by itself.

The paper is structured as follows: First, we describe the theoretical background and the implementation of the selected CI method with perturbative corrections. Then, we demonstrate the convergence for ground states of complexes of up to 13 excitons. Subsequently, we apply the method to the simulation of three-exciton emission spectra, and, after discussing

the role of single-particle basis states, we demonstrate how accurate calculations can be performed with a limited set of Coulomb matrix elements.

II. THEORY

A. Many-body Hamiltonian

The main goal of this paper is to assess the efficiency and applicability of a variant of the CIPSI algorithm for calculations of interacting carriers in quantum nanostructures. Neglecting Auger processes [55], which are strongly suppressed in gapped systems, the many-body Hamiltonian for interacting electrons and holes in a quantum nanostructure is

$$\begin{aligned} H = &\sum_i E_i^{(e)} c_i^\dagger c_i + \frac{1}{2}\sum_{ijkl}\langle ij|V_{ee}|kl\rangle c_i^\dagger c_j^\dagger c_k c_l \\ &+ \sum_p E_p^{(h)} h_p^\dagger h_p + \frac{1}{2}\sum_{pqrs}\langle pq|V_{hh}|rs\rangle h_p^\dagger h_q^\dagger h_r h_s \\ &- \sum_{iqrl}\left(\langle iq|V_{eh}^{\mathrm{dir}}|rl\rangle - \langle iq|V_{eh}^{\mathrm{exc}}|lr\rangle\right) c_i^\dagger h_q^\dagger h_r c_l, \end{aligned} \tag{1}$$

where $E_i^{(e)}$ and $E_p^{(h)}$ are the single-particle energy eigenvalues of the ith conduction band electron state and of the pth hole state (negative of the valence band electron energy eigenvalue), respectively, and $c_i^\dagger$ and $h_p^\dagger$ are the corresponding creation operators for electrons and holes. $\langle ij|V_{ee}|kl\rangle$, $\langle pq|V_{hh}|rs\rangle$, $\langle iq|V_{eh}^{\mathrm{dir}}|rl\rangle$, and $\langle iq|V_{eh}^{\mathrm{exc}}|lr\rangle$ are the electron-electron, hole-hole, as well as the direct and the exchange electron-hole Coulomb matrix elements, e.g.,

$$\begin{aligned} &\langle ij|V_{ee}|kl\rangle \\ &= \int d\mathbf{r}_1 \int d\mathbf{r}_2 \psi_i^*(\mathbf{r}_1)\psi_j^*(\mathbf{r}_2)V(\mathbf{r}_1,\mathbf{r}_2)\psi_k(\mathbf{r}_2)\psi_l(\mathbf{r}_1), \end{aligned} \tag{2}$$

where $V(\mathbf{r}_1,\mathbf{r}_2)$ describes the screened interaction potential between carriers at positions $\mathbf{r}_1$ and $\mathbf{r}_2$.

A general many-body state in a semiconductor nanostructure composed of n_e electrons and n_h holes can be described by

$$\begin{aligned} |\Psi\rangle = &\sum_{\substack{\{\mu_1,\ldots,\mu_{n_e};\\ \nu_1,\ldots,\nu_{n_h}\}}}{}' A\left(\mu_1,\ldots,\mu_{n_e};\nu_1,\ldots,\nu_{n_h}\right) \\ &\times c_{\mu_1}^\dagger \cdots c_{\mu_{n_e}}^\dagger h_{\nu_1}^\dagger \cdots h_{\nu_{n_h}}^\dagger |0\rangle, \end{aligned} \tag{3}$$

where μ_i and ν_i denote indices of electron and hole states, respectively, $|0\rangle$ is the semiconductor ground state with a full valence band and an empty conduction band, and A are expansion coefficients. The prime on the summation indicates that we sum only over indices with $\mu_i < \mu_{i+1}$ and $\nu_i < \nu_{i+1}$. A set of indices $\{\mu_1,\ldots,\mu_{n_e};\nu_1,\ldots,\nu_{n_h}\}$ with the constraints $\mu_i < \mu_{i+1}$ and $\nu_i < \nu_{i+1}$ defines a single configuration and all possible configurations together form a complete basis of the many-body Hilbert space $\mathcal{H}$. In order to keep the many-body Hilbert space finite, one typically only accounts for a finite number of N_e electron and N_h hole states.

The full CI method consists of constructing all possible configurations $c_{\mu_1}^\dagger \ldots c_{\mu_{n_e}}^\dagger h_{\nu_1}^\dagger \cdots h_{\nu_{n_h}}^\dagger|0\rangle$ in the expansion of $|\Psi\rangle$ in Eq. (3) for a given number of electrons n_e and holes n_h and for a given number of single-particle states N_e and N_h and then solving the eigenvalue equation $H|\Psi\rangle = \lambda|\Psi\rangle$ to obtain the eigenvalues λ and the eigenvectors in terms of the expansion coefficients A.

B. CIPSI method

In practice, the CI method is limited by the fact that the total dimension of the many-body Hilbert space $\mathcal{H}$ is given by $\binom{N_e}{n_e}\times\binom{N_h}{n_h}$, so that a full CI treatment is only possible for a small number of interacting carriers and single-particle states. One method to tackle the analogous problem in the context of molecular physics is the CIPSI method [49,56]. There, the Hamiltonian is diagonalized only in a small subspace $\mathcal{H}_0 \subset \mathcal{H}$ of the full many-body Hilbert space $\mathcal{H}$ corresponding to the most relevant states for the calculation. Which states are selected as part of the relevant subspace is decided iteratively by a criterion based on perturbation theory.

The CIPSI method has the advantage that it is a controlled approximation as there is a single convergence parameter, the threshold ξ, which defines the accuracy. In the limit $\xi \to 0$ the full CI method is obtained, but the number of selected states approaches $\dim(\mathcal{H})$. For finite ξ, only quantitatively important configurations are explicitly taken into account. Additionally, the states that are not selected are taken into account by second-order perturbative corrections to the energy, which significantly enhances the accuracy.

The algorithm is summarized in Table I: We start with an initial small subspace $\mathcal{H}_0$, possibly a single configuration, and diagonalize the many-body Hamiltonian in the subspace $\mathcal{H}_0$. The resulting eigenstates, which we denote by $|n^{(0)}\rangle$, together with all configurations $|k^{(0)}\rangle$ outside of $\mathcal{H}_0$ form a complete basis of the full many-body Hilbert space $\mathcal{H}$. In order to improve the accuracy of $|n^{(0)}\rangle$, we consider the interaction with the configurations $|k^{(0)}\rangle$ outside of $\mathcal{H}_0$ perturbatively. Recall that the first-order perturbative correction $|n^{(1)}\rangle$ to the approximate eigenstate $|n^{(0)}\rangle$ is

$$|n^{(1)}\rangle = \sum_k \xi_{nk}|k^{(0)}\rangle, \tag{4a}$$

$$\xi_{nk} = \frac{\langle k^{(0)}|H|n^{(0)}\rangle}{E_n^{(0)} - E_k^{(0)}}, \tag{4b}$$

where $E_n^{(0)}$ is the eigenvalue corresponding to the eigenstate $|n^{(0)}\rangle$ of the Hamiltonian in the subspace $\mathcal{H}_0$ and $E_k^{(0)} = \langle k^{(0)}|H|k^{(0)}\rangle$ is the diagonal energy of the configuration $|k^{(0)}\rangle$.

ξ_{nk} can be understood as the contribution from the configuration $|k^{(0)}\rangle$ to the eigenstates $|n\rangle$ of the full many-body Hamiltonian approximated by the state $|n^{(0)}\rangle$. Therefore, in the selected configuration interaction method CIPSI, a configuration $|k^{(0)}\rangle$ is considered to be important for a more accurate description of a target state $|n^{(0)}\rangle$ if $|\xi_{nk}|$ exceeds a given threshold value ξ. Thus, we loop through the configurations $|k^{(0)}\rangle$ outside of $\mathcal{H}_0$ and, if $|\xi_{nk}| > \xi$, we add the configuration $|k^{(0)}\rangle$ to the selected state space $\mathcal{H}_0$ for the next iteration. This process is repeated until no new configurations are selected, which typically requires five to ten iterations.

Note that, during the selection process, one already calculates all terms that enter the expression of the second-order

TABLE I. Layout of the CIPSI algorithm.

CIPSI Algorithm
(1) Start with an initial set of selected configurations $\mathcal{H}_0$.
(2) Diagonalize many-body Hamiltonian H in $\mathcal{H}_0$. Let $E_n^{(0)}$ be the nth eigenvalue and $\|n^{(0)}\rangle$ the corresponding eigenvector.
(3) For given target eigenstates $\|n^{(0)}\rangle$ and for configurations $\|k^{(0)}\rangle$ outside of the selected state space $\mathcal{H}_0$: Calculate $\xi_{nk} = \langle k^{(0)}\|H\|n^{(0)}\rangle/(E_n^{(0)} - E_k^{(0)})$.
(4) If $\|\xi_{nk}\| > \xi$: Add the configuration k to $\mathcal{H}_0$.
(5) Repeat from step (2) until no new states are added in step (4).
(6) Calculate the second-order perturbative corrections $\Delta E_{PT}^n = \sum_{k\notin\mathcal{H}_0} \|\langle k^{(0)}\|H\|n^{(0)}\rangle\|^2/(E_n^{(0)} - E_k^{(0)})$.

perturbative correction to the energy eigenvalues

$$\Delta E_{PT}^n = \sum_k \frac{\|\langle k^{(0)}|H|n^{(0)}\rangle\|^2}{E_n^{(0)} - E_k^{(0)}}, \tag{5}$$

so that the perturbative energy corrections, which will be shown to improve the convergence significantly, can be obtained with no additional numerical effort.

For large system sizes the numerically most demanding part of the algorithm is the calculation of $\langle k^{(0)}|H|n^{(0)}\rangle$ in step (3). This is due to the fact that the full many-body Hamiltonian H connects states from $\mathcal{H}_0$ to a much larger space, henceforth denoted by $\mathcal{H}_c$, which consists of all configurations obtained from configurations in $\mathcal{H}_0$ with additionally up to two excitations. In practice, storing a vector of configurations in the large connected space $\mathcal{H}_c$ is the limiting factor of the algorithm in terms of memory consumption.

Furthermore, the represention of a vector in the connected space $\mathcal{H}_c$ as a sparse vector in the full Hilbert space $\mathcal{H}$ requires searches in a list of size $\dim(\mathcal{H}_c)$. Because the lookup is critical for the performance of the algorithm, here, we implement it using hash tables, which have constant scaling $O(1)$ with respect to the length of the list, in contrast to, e.g., the search in an ordered list or in a binary tree that scales as $O[\log\dim(\mathcal{H}_c)]$ or a brute-force search of a state in a list of states without preordering which requires linear time in $\dim(\mathcal{H}_c)$.

The CIPSI algorithm described in Table I is formulated on the level of configurations, irrespective of the single-particle basis from which the configurations are constructed. However, the choice of the basis states may influence the convergence of the method. Due to the strong confinement in quantum nanostructures like quantum dots, here, we choose to work most of the time in the basis of eigenstates of a single-particle Hamiltonian that captures the details of the structure, such as the confinement potential, alloying, strain, and the underlying crystal lattice. In the present case, we use the $spds^*$ tight-binding Hamiltonian H_{TB} described in Appendix A, but other effective single-particle methods such as empirical pseudopotentials [54] might be used as well. Because in some scenarios CI calculations have been shown [42] to converge faster using a single-particle basis consisting of Hartree-Fock orbitals, we also test the convergence in the Hartree-Fock basis in a later section.

Finally, we note that the CIPSI method allows us to treat ground and excited states on the same footing. For example, for calculations of the lowest n_{EV} states, we use the same subspace $\mathcal{H}_0$ for all states. We diagonalize the Hamiltonian in the subspace $\mathcal{H}_0$, take the n_{EV} lowest eigenstates and add in step (4) of the algorithm all configurations $\|k^{(0)}\rangle$ to the selected state space for the next iteration if $\|\xi_{nk}\| > \xi$ for any $n \leqslant n_{EV}$.

III. RESULTS

We now test the CIPSI algorithm on the example of a hexagonal $InAs_{0.2}P_{0.8}$/InP nanowire quantum dot with a diameter of 18 nm and a height of 4 nm as depicted in Fig. 1(a). The single-particle states are obtained using the tight-binding model developed in Ref. [41] and briefly summarized in Appendix A. From the single-particle eigenstates in the representation as a linear combination of atomic orbitals, we calculate Coulomb matrix elements assuming a dielectrically screened Coulomb interaction

$$V(\mathbf{r}_1, \mathbf{r}_2) = \frac{e^2}{4\pi\epsilon_0\epsilon(\mathbf{r}_1, \mathbf{r}_2)} \frac{1}{\|\mathbf{r}_1 - \mathbf{r}_2\|}, \tag{6}$$

where the dielectric screening $\epsilon(\mathbf{r}_1, \mathbf{r}_2)$ is modeled by unscreened interactions $\epsilon = 1$ on the same atom and screening with a static dielectric constant $\epsilon = 12.4$ for long-range terms. In the many-body calculations, we account for up to $N_e = N_h = 40$ electron and hole states.

A. Convergence of excitonic ground states

The lowest-energetic many-body states for systems consisting of 1, 2, 3, 7, and 13 excitons calculated using the CIPSI method with (SCI + PT) and without (SCI) second-order perturbative corrections are depicted in Figs. 2(a)–2(e) as a function of the threshold ξ. Note that smaller values of ξ lead to the selection of more states and therefore correspond to results closer to full CI. The convergence with respect to ξ is qualitatively similar for most complexes, although the energy scales are different. To highlight the general features, we plot in Fig. 2(f) the CIPSI ground-state energies for all complexes up to 13 excitons normalized according to

$$E^{nX}_{\mathrm{normalized}}(\xi) = \frac{E^{nX}_{\mathrm{SCI+PT}}(\xi) - E^{nX}_{\mathrm{SCI+PT}}(\infty)}{\left|\Delta E^{nX}_{\mathrm{PT}}(\infty)\right|}. \tag{7}$$

Here, $E^{nX}_{\mathrm{SCI+PT}}(\xi) = E^{nX}_{\mathrm{SCI}}(\xi) + \Delta E^{nX}_{\mathrm{PT}}(\xi)$ is the result of a CIPSI calculation of the gound state of the complex comprised of n excitons for the threshold ξ including the perturbative correction $\Delta E^{nX}_{\mathrm{PT}}(\xi)$. The reference energy scale $|\Delta E^{nX}_{\mathrm{PT}}(\infty)|$ is given by the perturbative correction to the single configuration constructed from the lowest single-particle states, where no configurations are added in step (4) of the algorithm.

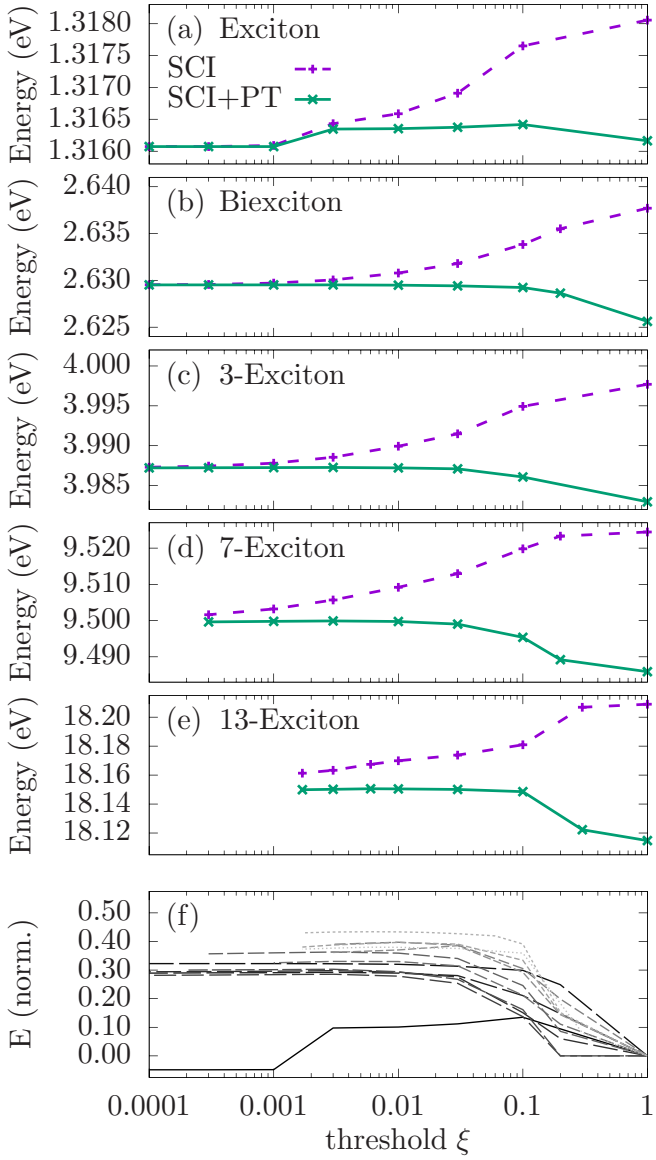

FIG. 2. Energies of the ground states of complexes comprised of 1 (a), 2 (b), 3 (c), 7 (d), and 13 (e) excitons as a function of the CIPSI threshold ξ. SCI (purple) denotes the energy eigenvalue of the many-body Hamiltonian projected onto the subspace of selected configurations; SCI + PT (green) includes the perturbative corrections from higher-energetic configurations. (f) shows the ground states from 1 to 13 excitons normalized according to Eq. (7), where brighter lines with shorter dashes correspond to larger complexes.

Except for the single exciton, for which the full Hilbert space is comparatively small with $\dim(\mathcal{H}) = 1600$, the different excitonic complexes converge with respect to the threshold ξ in a similar way. The energy increases and reaches a plateau at a threshold between $\xi = 0.1$ and $\xi = 0.01$. The value of the final energy indicates that the perturbative correction $|\Delta E^{nX}_{\mathrm{PT}}(\infty)|$ from a single configuration overestimates the influence of the remaining configurations by 30%–50%. The overestimation of the correction is a typical feature of perturbation theory in which higher-order corrections often have alternating signs.

In order to assess the efficiency of the CIPSI algorithm for quantum nanostructures, we plot in Fig. 3 the number of

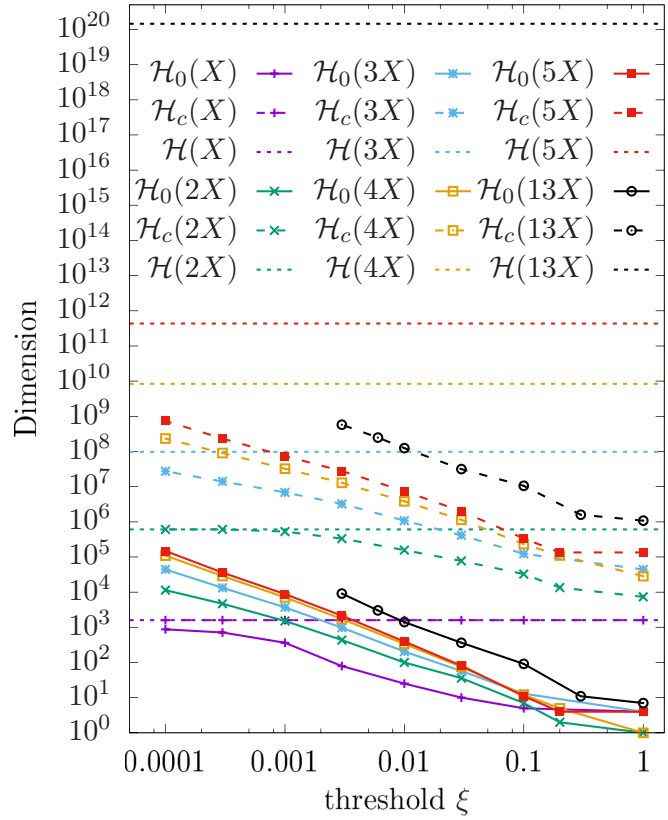

FIG. 3. Number of selected configurations $\dim(\mathcal{H}_0)$, dimension of connected space $\dim(\mathcal{H}_c)$, and dimension of the full many-body Hilbert space $\dim(\mathcal{H})$ constructed from 40 electron and hole states as a function of the threshold ξ for the ground-state calculation of excitonic complexes composed of 1 to 5 and 13 excitons.

selected states, i.e., the dimension of the subspace $\mathcal{H}_0$, the dimension of the connected subspace $\mathcal{H}_c$, which determines the memory consumption of the algorithm, and the dimension of the full many-body Hilbert space $\mathcal{H}$ constructed from up to 40 electron and hole states for calculations of excitonic complexes composed of 1 to 5 and of 13 excitons. We find that, except for the smallest complexes, the dimensions of the different spaces differ by many orders of magnitude. For example, for the five-exciton complex at a threshold of $\xi = 0.01$, one only has to diagonalize the many-body Hamiltonian in a space with dimension $\dim(\mathcal{H}_0) \approx 400$ while perturbative corrections due to 7.4×10^6 other configurations have to be performed out of the total many-body Hilbert space with the dimension $\dim(\mathcal{H}) \approx 4.3\times10^{11}$. It is noteworthy that, although the full many-body Hilbert space grows very fast with the number of particles (about two orders of magnitude when one additional exciton is added), the number of selected states as well as the dimension of the connected Hilbert space, which limits the calculations, increase much more slowly. Therefore, the CIPSI algorithm is particularly useful for systems with a large number of particles.

B. Convergence of optical spectra

So far, we have only considered the convergence of the selected CI algorithm for ground states, but it can equally

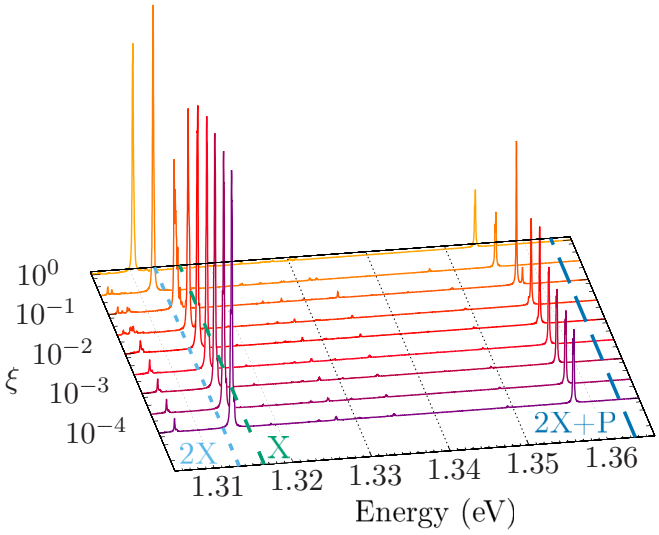

FIG. 4. Spectral lines emitted from the three-exciton complex for different thresholds ξ. Additionally indicated are the positions of the lowest bright exciton (X) and biexciton ($2X$) lines as well as the biexciton transtion energy shifted by electron and hole s-p-shell splittings ($2X + P$).

well be used to calculate excited states. This enables, e.g., calculations of emission spectra from higher excitonic complexes. The spectroscopy of the three-exciton complex is particularly interesting, as already the lowest three-exciton state requires the occupation of p-shell electron and hole states, whereas emission from single excitons and biexcitons after thermalization predominantly originates from s-shell states. Therefore, from the spectral lines emitted by the three-exciton complex one can infer information about the quantization and lateral confinement in quantum nanostructures. Although due to thermalization only a small number of three-exciton states contribute to the spectrum, the simulation of transitions in the spectral range that contains three-exciton emission from the s shell as well as from the p shell is a good testing ground for selected CI calculations of excited states, as it requires the calculation of a large number of excited biexciton states.

In Fig. 4, the accumulated three-exciton emission spectrum for all polarization directions (cf. Appendix B for details on definition and computation) is depicted for different values of the threshold ξ in a spectral region that captures emission from s- and p-shell states. The many-body eigenstates for both initial three-exciton states and final biexciton states are calculated using the selected CI algorithm and we add perturbative corrections to the respective energy eigenvalues. As reference points we also mark the spectral positions of the bright emission lines for the s-shell exciton-to-ground-state (X) and biexciton-to-exciton ($2X$) transitions obtained from full CI calculations. In addition, we indicate the energy obtained by adding the splittings between the lowest s and p shells for electrons and holes $\Delta E_p = [E^{(e)}_{1p} - E^{(e)}_{1s}] + [E^{(h)}_{1p} - E^{(h)}_{1s}]$ to the position of the biexciton-to-exciton transition ($2X + P$).

Two peaks dominate the three-exciton spectra, one close to the lowest exciton transition, which corresponds to recombination of s-shell electrons with s-shell holes, and one that is shifted by approximately the s-p splitting ΔE_p, which stems from the recombination of p-shell electrons with p-shell holes. Additionally, a number of very small peaks in the spectrum indicate dark states that are optically forbidden either due to spatial symmetries, such as recombination from p-shell electrons with s-shell holes, or spin selection rules. Here, we find that the s-shell three-exciton transition line is found between the biexciton and exciton lines. Furthermore, the distance between the two main peaks in the three-exciton spectrum 43.6 meV is about 13% smaller than the sum of the electron and hole s-p splittings $\Delta E_p = 50.3$ meV. We attribute this significant deviation from the single-particle picture to the fact that the spectral proximity of nearly degenerate p orbitals makes it easier to reorganize charge densities to minimize Coulomb repulsion, so that the many-body contribution to biexcitons with p-shell carriers can be reduced compared to biexcitons with only s-shell carriers. This finding implies that s-p splittings and confinement energies are typically underestimated when they are derived from the distance between three-exciton emission lines.

Regarding the convergence of the selected CI algorithm we find that, similar to the case of ground states of excitonic complexes discussed earlier, the spectra are well converged at $\xi = 0.01$. Furthermore, note that, in order to fully capture the s-shell emission peak, more than 60 biexciton states have to be calculated. To this end, calculations of the 120 lowest biexciton states have been performed. As we work with a single selected state space $\mathcal{H}_0$ for ground and excited states, a larger number of states are selected when 120 states are requested compared with the calculation of only the ground state. For smaller values of the threshold ξ, however, the ratio between the number of selected states in both cases is more and more reduced and is found to be $\sim$10 for $\xi = 10^{-4}$.

It is also noteworthy that we can make use of synergies in the calculation of multiple eigenstates: The approximate eigenstates $|n^{(0)}\rangle = \sum_i \alpha_{ni}|i\rangle$ are stored as linear combinations of single configurations $|i\rangle \in \mathcal{H}_0$. Then, the off-diagonal matrix elements required in step (3) of the algorithm are calculated by $\langle k^{(0)}|H|n^{(0)}\rangle = \sum_i \alpha_{ni}\langle k^{(0)}|H|i\rangle$. For different eigenstates, only the coefficients α_{ni} change, but the numerically costly matrix elements in terms of single configurations $\langle k^{(0)}|H|i\rangle$ have to be calculated only once. Therefore, calculating more eigenstates only leads to a marginal increase in computation time, which makes the selected CI in practice very efficient for the calculation of a large number of eigenstates, as long as enough memory for the simultaneous storage of ξ_{nk} is available.

C. CIPSI in Hartree-Fock basis

In quantum dots charged with many electrons, it was shown [42] that CI calculations converge faster with the number of single-particle states when configurations are constructed from Hartree-Fock single-particle states instead of eigenstates of a single-particle Hamiltonian. This is due to the fact that Hartree-Fock calculations already capture the redistribution of charge densities due to Coulomb repulsion. To investigate whether also the convergence of the CIPSI method can be enhanced by working in the Hartree-Fock basis, we present in Fig. 5 the absolute error $|E_{\mathrm{CIPSI}} - E_{\mathrm{CI}}|$ of the CIPSI algorithm

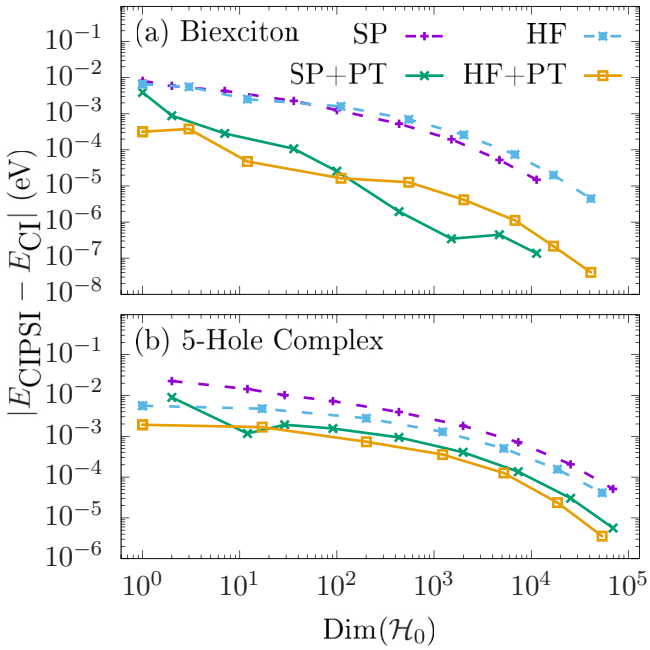

FIG. 5. Convergence of CIPSI calculations in the basis of single-particle eigenstates compared with calculations starting from the Hartree-Fock basis for (a) the lowest biexciton and (b) the lowest-energetic complex composed of five holes. The absolute error with respect to a full CI calculation is shown as a function of the number of selected states on a double-logarithmic scale.

with respect to the full CI calculation of the lowest biexciton state [Fig. 5(a)] and of the ground state of a many-body system comprised of five holes [Fig. 5(b)] as a function of the number of selected states dim($\mathcal{H}_0$) for calculations in the basis of eigenstates of the single-particle Hamiltonian (SP) as well as in the Hartree-Fock basis (HF) with and without perturbative corrections (PT).

For the highly charged five-hole complex, the calculation in the Hartree-Fock basis indeed generally leads to a smaller error for the same number of selected states. However, the errors in both bases are of the same order of magnitude, in particular when more than a few states $\gtrsim$10 are selected. For the biexciton state, the first data point corresponds to a single configuration comprised of two electrons and two holes in the lowest s shells. The energy of this state in the basis of eigenstates of the single-particle Hamiltonian is ∼8.2 meV above the full CI value taking into account 40 electron and holes states while a Hartree-Fock optimization of single-particle states reduces this value to ∼6.6 meV. It is noteworthy that including perturbative corrections to the single s-shell configuration in the basis of single-particle eigenstates already yields a more accurate result than the Hartree-Fock calculation without corrections. With perturbative corrections, the respective Hartree-Fock state is found to be even more accurate by one order of magnitude. Thus, the Hartree-Fock basis has a slight advantage over the single-particle Hamiltonian eigenstates when only a few states are selected. However, reducing the threshold to select more states, we find that at $\gtrsim$100 states the single-particle eigenstates become more favorable for convergence and the additional Hartree-Fock step required for the calculation is eventually detrimental.

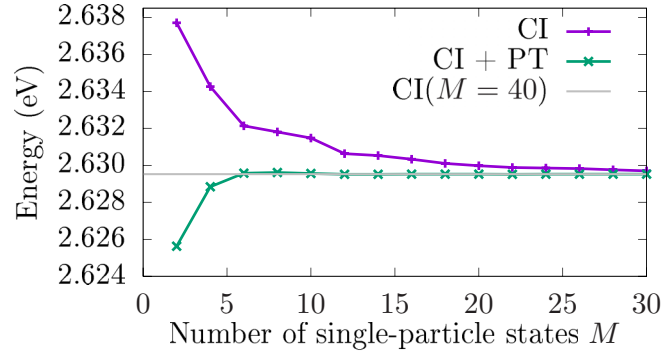

FIG. 6. Full CI calculation of the lowest biexciton state using M single-particle states with and without perturbative correction in the Hilbert space of up to 40 single-particle states.

D. Reduced number of Coulomb matrix elements

As we have shown so far, the CIPSI algorithm reduces the numerical demands for calculations of the many-body states of interacting carriers in quantum dots significantly compared to full CI calculations. However, for practical purposes, a major problem that remains is the calculation of Coulomb matrix elements. This is due to the fact that the number of matrix elements, e.g., of $\langle ij|V_{ee}|kl\rangle$, scales as $O(N^4)$ with the number of single-particle states that are accounted for in the calculation. Furthermore, even when only two-center terms are taken into account, the calculation of a single Coulomb matrix element scales as $O(N_{\mathrm{at}}^2)$ with the number of atoms N_{at}. Therefore, the numerical demands of the calculation of Coulomb matrix element often limit the overall accuracy of the calculation. One approach to attack this problem is linear scaling methods [57] with respect to N_{atoms} to reduce the calculation time for a single matrix element. Alternatively, one can speed up the calculation by vectorization [58] or parallelization [41].

Here, in light of the effectiveness of perturbative corrections, we propose another way to reduce the numerical demands for the calculation of Coulomb matrix elements: Calculating many-body states in a restricted Hilbert space consisting of at most M single-particle states per band and adding the effects of a much larger Hilbert space with up to N single-particle states perturbatively requires only the knowledge of matrix elements, e.g., $\langle ij|V_{ee}|kl\rangle$ with $i, j \leqslant N$ and $k, l \leqslant M$. Thus, as long as the influence of configurations containing states $i > M$ is well described by perturbation theory, one only needs to calculate $O(N^2M^2)$ instead of $O(N^4)$ Coulomb matrix elements.

In Fig. 6 we show the results of full CI calculations of the lowest-energy biexciton states in a Hilbert space with up to M single-particle states per band. Then, we add perturbative corrections from higher-lying states with up to $N = 40$ single-particle states per band (CI + PT). It turns out that the calculation is practically converged at $M = 6$ states when perturbative corrections are included. Note that in this case only about $(M/N)^2 \sim 2\%$ of all possible Coulomb matrix elements from $N = 40$ single-particle states had to be used. Therefore, using perturbative corrections not only speeds up the calculation of many-body states, but also allows for a drastic reduction of the computational resources for the Coulomb

matrix element calculation without significantly reducing the overall accuracy.

IV. CONCLUSION

We have presented a selected configuration interaction method with perturbative corrections that enables highly accurate and efficient calculations of many-body states of interacting charge carriers in quantum nanostructures. This method has a number of advantages: It is controlled by a single convergence parameter ξ and yields full CI results in the limit $\xi \to 0$; it is applicable in very general settings without requiring special conditions like symmetries; it also allows an efficient calculation of excited states, and reduces the computational effort for obtaining Coulomb matrix elements. The fast convergence is demonstrated numerically for the ground states of complexes comprised of up to 13 excitons. We find that the calculations are typically converged for thresholds ξ between 0.01 and 0.1 and within about five to ten iterative state selection steps. A similar convergence is found of excited states, which we have tested by calculating the emission spectra from three-exicton complexes. Finally, we have analyzed the choice of single-particle states and we have demonstrated a method for accurate many-body calculations with a significantly reduced number of Coulomb matrix elements.

Our investigations show that, due to its extreme efficiency and accuracy, the selected configuration interaction method with perturbative corrections can serve as a general purpose tool for the calculation of many-body states of interacting carriers in quantum nanostructures and it can yield quantitatively accurate results in cases far out of reach for full configuration interaction calculations. However, it is noteworthy that there exist optimized variants of the CIPSI method in the context of quantum chemistry [59] that are even more efficient and it will be interesting to investigate and analyze their implementations for quantum nanostructure in the future. In particular, the heat-bath CI variant [51–53,60] offers great potential for accelerating the state selection process by using a different selection criterion. There, configurations k are selected if $|\langle k|H|i\rangle c_i| < \epsilon$ for any i, where i and k are single configurations, c_i is the expansion coefficient of the target eigenstate in terms of the configuration i, and ϵ is an energy threshold. This criterion has the advantage that by presorting the matrix elements a large number of noncontributing terms can be dropped in advance and do not have to be sampled explicitly. This paves the way for simulations of even larger systems of correlated electrons in quantum nanostructures.

ACKNOWLEDGMENTS

M.C. gratefully acknowledges funding from the Alexander von Humboldt Foundation through a Feodor-Lynen research fellowship. M.C. and P.H. acknowledge support from NSERC QC2DM Project and uOttawa Chair in Quantum Theory of Materials, Nanostructures and Devices. This work was performed, in part, at the Center for Nanoscale Materials, a U.S. Department of Energy Office of Science User Facility, and supported by the U.S. Department of Energy, Office of Science, under Contract No. DE-AC02-06CH11357. P.H. and M.C. acknowledge computational resources provided by Compute Canada and by the Center for Nanoscale Materials.

APPENDIX A: TIGHT-BINDING DESCRIPTION OF SINGLE-PARTICLE STATES

The description of many-body complexes is based on interacting carriers on a basis of single-particle states. To test the CIPSI method, we choose to work with a concrete example of single-particle eigenstates of an InAsP nanowire quantum dot [12]. An atomistic tight-binding description for such systems was derived from first principles in Ref. [41] and implemented within our computational toolkit QNANO [5,32,41,61] suitable for large-scale parallelized million-atom calculations on a computer cluster.

At the core of the calculation of single-particle states is a description in terms of the tight-binding Hamiltonian

$$H_{\mathrm{TB}} = \sum_{i=1}^{N_{\mathrm{at}}} \sum_{\alpha=1}^{N_{\mathrm{orb}}} \epsilon_{i,\alpha} \tilde{c}^{\dagger}_{i,\alpha} \tilde{c}_{i,\alpha} + \sum_{i=1}^{N_{\mathrm{at}}} \sum_{\alpha,\beta=1}^{N_{\mathrm{orb}}} \lambda_{i,\alpha,\beta} \tilde{c}^{\dagger}_{i,\alpha} \tilde{c}_{i,\beta} + \sum_{i=1}^{N_{\mathrm{at}}} \sum_{j=1}^{nn(i)} \sum_{\alpha,\beta=1}^{N_{\mathrm{orb}}} t_{i,\alpha,j,\beta} \tilde{c}^{\dagger}_{i,\alpha} \tilde{c}_{j,\beta}, \tag{A1}$$

where $\tilde{c}^{\dagger}_{i,\alpha}$ is the creation operator for an electron in the local orbital α on atom i. N_{at} is the number of atoms in the sample and we use an $spds^*$ model with $N_{\mathrm{orb}} = 20$ orbitals per atom. $\epsilon_{i,\alpha}$ are the on-site energies, $t_{i,\alpha,j,\beta}$ are the nearest-neighbor hopping elements from orbital α on atom i to orbital β on atom j, and $\lambda_{i,\alpha,\beta}$ describes the spin-orbit coupling at atom i. To account for strain, the on-site and hopping parameters are modified based on the local bond lengths and angles, which we obtain by performing a valence-force-field strain relaxation. A detailed description of the tight-binding parameters and strain corrections is given in Ref. [41]. The tight-binding Hamiltonian H_{TB} is diagonalized, which yields the energy eigenvalues as well as the single-particle eigenstates $\psi_i(\mathbf{r})$ in terms of expansion coefficients $C(i,k,\alpha)$ of a linear combination of atomic orbitals $\varphi_\alpha(\mathbf{r} - \mathbf{R}_k)$,

$$\psi_i = \sum_{k=1}^{N_{\mathrm{at}}} \sum_{\alpha=1}^{N_{\mathrm{orb}}} C(i,k,\alpha) \varphi_\alpha(\mathbf{r} - \mathbf{R}_k), \tag{A2}$$

where $\mathbf{R}_k$ is the position of atom k.

APPENDIX B: CALCULATION OF OPTICAL EMISSION SPECTRA

The optical emission spectrum of an excitonic complex can be described by Fermi's golden rule. The intensity of the emitted light with polarization direction $\boldsymbol{\epsilon}$ is [41]

$$F(E,\boldsymbol{\epsilon}) = F_0 \sum_{i,f} |\langle i|P(\boldsymbol{\epsilon})|f\rangle|^2 \delta[E - (E_f - E_i)] n_i (1 - n_f), \tag{B1}$$

where i and f denote the initial and final many-body states, E_i and E_f are the respective energies, $\langle i|P(\boldsymbol{\epsilon})|f\rangle$ is the dipole matrix element between states i and f, n_i and n_f are the occupations of the initial and final states, and F_0 is a constant depending on the light-matter interaction.

Here, we calculate the emission spectrum from three-exciton complexes to biexciton states, where we assume empty final states $n_f = 0$ and a thermal distribution of the

initial three-exciton states at a temperature $T = 4$ K. The δ functions in Eq. (B1) are broadened to Lorentzians with a phenomenological linewidth of 0.1 meV. The dipole matrix elements are calculated from the many-body eigenstates

$$\begin{aligned}\langle i|P(\boldsymbol{\epsilon})|f\rangle &= \sum_{\mu'=1}^{N_e}\sum_{\nu'=1}^{N_h}\langle i|c^\dagger_{\mu'}h^\dagger_{\nu'}|f\rangle\langle\psi_{\mu'}|\boldsymbol{\epsilon}\cdot\mathbf{r}|\psi_{\nu'}\rangle \\ &= \sum_{\mu'=1}^{N_e}\sum_{\nu'=1}^{N_h}\langle\psi_{\mu'}|\boldsymbol{\epsilon}\cdot\mathbf{r}|\psi_{\nu'}\rangle \\ &\quad\times \sum_{\substack{\{\mu_1,\ldots,\mu_{n_e};\\ \nu_1,\ldots,\nu_{n_h}\}}}{}' A^{i*}(\mu_1,\ldots,\mu',\ldots,\mu_{n_e}; \\ &\qquad \nu_1,\ldots,\nu',\ldots,\nu_{n_h}) \\ &\quad\times A^f(\mu_1,\ldots,\mu_{n_e};\nu_1,\ldots,\nu_{n_h}),\end{aligned} \tag{B2}$$

where A^i and A^j are the many-body eigenstate expansion coefficients as in Eq. (3). The dipole matrix elements $\langle\psi_{\mu'}|\boldsymbol{\epsilon}\cdot\mathbf{r}|\psi_{\nu'}\rangle$ between valence and conduction band single-particle states $\psi_{\nu'}$ and $\psi_{\mu'}$ are obtained in the representation Eq. (A2) in terms of local atomic orbitals

$$\langle\psi_{\mu'}|\boldsymbol{\epsilon}\cdot\mathbf{r}|\psi_{\nu'}\rangle = \sum_{k=1}^{N_{\mathrm{at}}}\sum_{\alpha=1}^{N_{\mathrm{orb}}} C^*(\mu',k,\alpha)C(\nu',k,\alpha)\mathbf{R}_k. \tag{B3}$$

Note that we use local atomic orbitals with defined spin states, so that spin selection rules are automatically included via the orthogonality relations used in the derivation of Eq. (B3).

Here, we are interested in the total emission of excitonic complexes including all polarization directions. To this end we add the emitted light $F(E) = F(E,\mathbf{e}_x) + F(E,\mathbf{e}_y) + F(E,\mathbf{e}_z)$ with polarizations along the three spatial coordinates with unit vectors $\mathbf{e}_x$, $\mathbf{e}_y$, and $\mathbf{e}_z$.

[1] L. Jacak, P. Hawrylak, and A. Wojs, *Quantum Dots* (Springer-Verlag, Berlin/Heidelberg, 1998).

[2] P. Hawrylak and M. Korkusinski, in *Single Quantum Dots: Fundamentals, Applications, and New Concepts* (Springer-Verlag, Berlin/Heidelberg, 2003), pp. 25–92.

[3] Y. Arakawa and H. Sakaki, Appl. Phys. Lett. **40**, 939 (1982).

[4] S. M. Reimann and M. Manninen, Rev. Mod. Phys. **74**, 1283 (2002).

[5] N. F. Hartmann, M. Otten, I. Fedin, D. Talapin, M. Cygorek, P. Hawrylak, M. Korkusinski, S. Gray, A. Hartschuh, and X. Ma, Nat. Commun. **10**, 3253 (2019).

[6] E. V. Shornikova, D. R. Yakovlev, L. Biadala, S. A. Crooker, V. V. Belykh, M. V. Kochiev, A. Kuntzmann, M. Nasilowski, B. Dubertret, and M. Bayer, Nano Lett. **20**, 1370 (2020).

[7] P. Michler, A. Kiraz, C. Becher, W. V. Schoenfeld, P. M. Petroff, L. Zhang, E. Hu, and A. Imamoglu, Science **290**, 2282 (2000).

[8] M. Cosacchi, F. Ungar, M. Cygorek, A. Vagov, and V. M. Axt, Phys. Rev. Lett. **123**, 017403 (2019).

[9] C. Santori, M. Pelton, G. Solomon, Y. Dale, and Y. Yamamoto, Phys. Rev. Lett. **86**, 1502 (2001).

[10] A. Orieux, M. A. M. Versteegh, K. D. Jöns, and S. Ducci, Rep. Prog. Phys. **80**, 076001 (2017).

[11] R. M. Stevenson, R. J. Young, P. Atkinson, K. Cooper, D. A. Ritchie, and A. J. Shields, Nature (London) **439**, 179 (2006).

[12] M. A. M. Versteegh, M. E. Reimer, K. D. Jöns, D. Dalacu, P. J. Poole, A. Gulinatti, A. Giudice, and V. Zwiller, Nat. Commun. **5**, 5298 (2014).

[13] A. Fognini, A. Ahmadi, M. Zeeshan, J. T. Fokkens, S. J. Gibson, N. Sherlekar, S. J. Daley, D. Dalacu, P. J. Poole, K. D. Jöns, V. Zwiller, and M. E. Reimer, ACS Photon. **6**, 1656 (2019).

[14] M. Bayer, P. Hawrylak, K. Hinzer, S. Fafard, M. Korkusinski, Z. R. Wasilewski, O. Stern, and A. Forchel, Science **291**, 451 (2001).

[15] M. Świderski and M. Zieliński, Phys. Rev. B **100**, 235417 (2019).

[16] M. Świderski and M. Zieliński, Phys. Rev. B **95**, 125407 (2017).

[17] P. Karwat, K. Gawarecki, and P. Machnikowski, Phys. Rev. B **95**, 235421 (2017).

[18] D. Kim, S. G. Carter, A. Greilich, A. S. Bracker, and D. Gammon, Nat. Phys. **7**, 223 (2011).

[19] M. D. Shulman, O. E. Dial, S. P. Harvey, H. Bluhm, V. Umansky, and A. Yacoby, Science **336**, 202 (2012).

[20] M. Russ, D. M. Zajac, A. J. Sigillito, F. Borjans, J. M. Taylor, J. R. Petta, and G. Burkard, Phys. Rev. B **97**, 085421 (2018).

[21] M. Russ and G. Burkard, J. Phys.: Condens. Matter **29**, 393001 (2017).

[22] M. Ediger, G. Bester, A. Badolato, P. M. Petroff, K. Karrai, A. Zunger, and R. J. Warburton, Nat. Phys. **3**, 774 (2007).

[23] H. Drexler, D. Leonard, W. Hansen, J. P. Kotthaus, and P. M. Petroff, Phys. Rev. Lett. **73**, 2252 (1994).

[24] R. J. Warburton, C. Schäflein, D. Haft, F. Bickel, A. Lorke, K. Karrai, J. M. Garcia, W. Schoenfeld, and P. M. Petroff, Nature (London) **405**, 926 (2000).

[25] D. V. Regelman, E. Dekel, D. Gershoni, E. Ehrenfreund, A. J. Williamson, J. Shumway, A. Zunger, W. V. Schoenfeld, and P. M. Petroff, Phys. Rev. B **64**, 165301 (2001).

[26] A. Wojs and P. Hawrylak, Phys. Rev. B **53**, 10841 (1996).

[27] M. Korkusinski, P. Hawrylak, and M. Potemski, J. Phys.: Condens. Matter **20**, 454213 (2008).

[28] M. Bayer, O. Stern, P. Hawrylak, S. Fafard, and A. Forchel, Nature (London) **405**, 923 (2000).

[29] S. Raymond, S. Fafard, P. J. Poole, A. Wojs, P. Hawrylak, S. Charbonneau, D. Leonard, R. Leon, P. M. Petroff, and J. L. Merz, Phys. Rev. B **54**, 11548 (1996).

[30] A. Hartmann, Y. Ducommun, E. Kapon, U. Hohenester, and E. Molinari, Phys. Rev. Lett. **84**, 5648 (2000).

[31] M. Cygorek, F. Ungar, T. Seidelmann, A. M. Barth, A. Vagov, V. M. Axt, and T. Kuhn, Phys. Rev. B **98**, 045303 (2018).

[32] M. Zieliński, M. Korkusiński, and P. Hawrylak, Phys. Rev. B **81**, 085301 (2010).

[33] N. Chauvin, E. Tranvouez, G. Bremond, G. Guillot, C. Bru-Chevallier, E. Dupuy, P. Regreny, M. Gendry, and G. Patriarche, Nanotechnology **17**, 1831 (2006).

[34] M. Holtkemper, D. E. Reiter, and T. Kuhn, Phys. Rev. B **97**, 075308 (2018).

[35] J. Kettler, M. Paul, F. Olbrich, K. Zeuner, M. Jetter, P. Michler, M. Florian, C. Carmesin, and F. Jahnke, Phys. Rev. B **94**, 045303 (2016).
[36] N. H. Lindner and T. Rudolph, Phys. Rev. Lett. **103**, 113602 (2009).
[37] I. Schwartz, D. Cogan, E. R. Schmidgall, Y. Don, L. Gantz, O. Kenneth, N. H. Lindner, and D. Gershoni, Science **354**, 434 (2016).
[38] R. Raussendorf, D. E. Browne, and H. J. Briegel, Phys. Rev. A **68**, 022312 (2003).
[39] B. Jaworowski, N. Rogers, M. Grabowski, and P. Hawrylak, Sci. Rep. **7**, 5529 (2017).
[40] M. Korkusinski, O. Voznyy, and P. Hawrylak, Phys. Rev. B **82**, 245304 (2010).
[41] M. Cygorek, M. Korkusinski, and P. Hawrylak, Phys. Rev. B **101**, 075307 (2020).
[42] R. M. Abolfath and P. Hawrylak, J. Chem. Phys. **125**, 034707 (2006).
[43] A. Wensauer, M. Korkusiński, and P. Hawrylak, Solid State Commun. **130**, 115 (2004).
[44] A. Wojs and P. Hawrylak, Solid State Commun. **100**, 487 (1996).
[45] R. J. Bartlett and M. Musiał, Rev. Mod. Phys. **79**, 291 (2007).
[46] F. Verstraete and J. I. Cirac, Phys. Rev. B **73**, 094423 (2006).
[47] L.-H. Frahm and D. Pfannkuche, J. Chem. Theory Comput. **15**, 2154 (2019).
[48] V. Abraham and N. J. Mayhall, arXiv:2002.03107.
[49] B. Huron, J. P. Malrieu, and P. Rancurel, J. Chem. Phys. **58**, 5745 (1973).
[50] M. Dash, S. Moroni, A. Scemama, and C. Filippi, J. Chem. Theory Comput. **14**, 4176 (2018).
[51] A. D. Chien, A. A. Holmes, M. Otten, C. J. Umrigar, S. Sharma, and P. M. Zimmerman, J. Phys. Chem. A **122**, 2714 (2018).
[52] J. Li, M. Otten, A. A. Holmes, S. Sharma, and C. J. Umrigar, J. Chem. Phys. **149**, 214110 (2018).
[53] J. Li, Y. Yao, A. A. Holmes, M. Otten, Q. Sun, S. Sharma, and C. J. Umrigar, Phys. Rev. Res. **2**, 012015 (2020).
[54] G. Bester, S. Nair, and A. Zunger, Phys. Rev. B **67**, 161306(R) (2003).
[55] M. Korkusinski, O. Voznyy, and P. Hawrylak, Phys. Rev. B **84**, 155327 (2011).
[56] R. Cimiraglia and M. Persico, J. Comput. Chem. **8**, 39 (1987).
[57] P. T. Różański and M. Zieliński, Phys. Rev. B **94**, 045440 (2016).
[58] W. Sheng, S.-J. Cheng, and P. Hawrylak, Phys. Rev. B **71**, 035316 (2005).
[59] N. M. Tubman, J. Lee, T. Y. Takeshita, M. Head-Gordon, and K. B. Whaley, J. Chem. Phys. **145**, 044112 (2016).
[60] J. E. T. Smith, B. Mussard, A. A. Holmes, and S. Sharma, J. Chem. Theory Comput. **13**, 5468 (2017).
[61] M. Korkusinski, in *Nanoscale Materials and Devices for Electronics, Photonics and Solar Energy*, edited by A. Korkin, S. Goodnick, and R. Nemanich (Springer International Publishing, Cham, 2015), pp. 149–216.